Clinical, Genetic and Structural Basis of Apparent Mineralocorticoid Excess Due to 11β-Hydroxysteroid Type 2 Deficiency

Mabel Yau[1^], Shozeb Haider[2^], Ahmed Khattab[1], Chen Ling[2], Mehr Mathew[1], Samir Zaidi[3], Madison Bloch[1], Monica Patel[1], Sinead Ewert[2], Wafa Abdullah[4], Aysenur Toygar[1], Vitalii Mudryi[2], Maryam Al Badi[4], Mouch Alzubdi[2], Robert C. Wilson[5], Hanan Said Al Azkawi[4], Hatice Nur Ozdemir[1], Wahid Abu-Amer[1], Jozef Hertecant[6], Maryam Razzaghy-Azar[7], John W. Funder[8], Aisha Al Senani[4], Li Sun[1], Se-Min Kim[1], Tony Yuen[1#], Mone Zaidi[1#], Maria I. New[1#]

[1]Departments of Medicine and Pediatrics, Icahn School of Medicine at Mount Sinai, New York, NY 10029, USA; and [2]Department of Pharmaceutical and Biological Chemistry, University College London School of Pharmacy, London WC1N 1AX, UK; [3]Department of Medicine, Massachusetts General Hospital, Harvard Medical School, Boston MA 02114, USA; [4]Department of Pediatrics, Royal Hospital, Muscat, Oman, [5]Department of Pathology and Laboratory Medicine, Medical University of South Carolina, Charleston, SC 29425; [6]Department of Pediatrics, Tawam Hospital, Abu Dhabi, United Arab Emirates; [7]Metabolic Disorders Research Center, Tehran University of Medical Sciences, Tehran, Iran; [8]Department of Medicine, Monash University, Clayton, VIC 3800, Australia. ([^]Joint First Authors, [#]Joint Senior Authors)

Correspondence to: mone.zaidi@mssm.edu (Tel: 212-241-8797) and maria.new@mssm.edu (Tel: 212-241-8747)

Key Words: *In Silico* molecular modeling; molecular dynamics; hypertension; congenital adrenal hyperplasia

SIGNIFICANCE STATEMENT

Apparent mineralocorticoid excess (AME), a rare autosomal recessive disorder characterized by low renin hypertension, may display a severe or mild phenotype in patients. The variability in clinical presentation stems from different extents of impairment of the 11β-hydroxysteroid dehydrogenase type 2 (HSD11B2) enzyme arising from distinct mutations in the encoding gene. The computational model of the HSD11B2 protein that we constructed here will be useful in predicting disease severity for newly reported missense mutations in this gene.

ABSTRACT

Mutations in 11β-hydroxysteroid dehydrogenase type 2 gene (*HSD11B2*) cause an extraordinarily rare autosomal recessive disorder, apparent mineralocorticoid excess (AME). AME is a form of low renin hypertension that is potentially fatal if untreated. Mutations in the *HSD11B2* gene result either in severe AME or a milder phenotype (type II AME). To date, ~40 causative mutations have been identified. As part of the International Consortium for Rare Steroid Disorders, we have diagnosed and followed the largest single worldwide cohort of 36 AME patients. Here, we present the genotype and clinical phenotype of these patients, prominently from consanguineous marriages in the Middle East, who display profound hypertension and hypokalemic alkalosis. To correlate mutations with phenotypic severity, we constructed a computational model of the HSD11B2 protein. Having used a similar strategy for the *in silico* evaluation of 150 mutations of *CYP21A2*, the disease causing gene in congenital adrenal hyperplasia, we now provide a full structural explanation for the clinical severity of AME resulting from each known *HSD11B2* missense mutation. We find that mutations that allow the formation of an inactive dimer, alter substrate/coenzyme binding, or impair structural stability of HSD11B2 yield severe AME. In contrast, mutations that cause an indirect disruption of substrate binding or mildly alter intramolecular interactions result in type 2 AME. A simple *in silico* evaluation of novel missense mutations could help predict the often-diverse phenotypes of an extremely rare monogenic disorder.

/body

INTRODUCTION

Apparent Mineralocorticoid Excess (AME) is an ultra-rare autosomal recessive disorder caused by a mutation in the 11β-hydroxysteroid dehydrogenase type 2 gene (*HSD11B2*), which leads to a deficiency in the HSD11B2 enzyme. HSD11B2, a member of the short chain alcohol dehydrogenase family, catalyzes the NAD^+-dependent dehydrogenation of cortisol. In the kidney, HSD11B2 converts cortisol to inactive cortisone. This mechanism protects the mineralocorticoid receptor from cortisol action, notwithstanding an equal *in vitro* affinity of the mineralocorticoid receptor for cortisol and aldosterone, and the 100- to 1000-fold higher circulating levels of cortisol (1, 2).

In 1977, we described the biochemical phenotype of a patient with AME (3). We found that, in the absence of HSD11B2, the mineralocorticoid receptor was occupied and stimulated by excess cortisol leading to hypertension without elevated aldosterone or renin levels. AME patients display low birth weight, failure to thrive, low-renin hypertension, and hypokalemia. Defective metabolism of cortisol to cortisone leads to the pathognomonic elevation in the ratio of urinary tetrahydrocortisol (THF) plus allo-THF to tetrahydrocortisone (THE) [(THF+alloTHF)/THE].

In a disorder in which one of the cardinal clinical features is hypertension, insidious end organ damage in renal, neurological, neuromuscular, cardiovascular, and ocular systems may arise at an early age from chronic elevation of blood pressure or through metabolic alkalosis and severe hypokalemia leading to renal disease. Cardiac failure resulting from hypokalemia, hypertensive crises, stroke, cardiomegaly, hypertensive retinopathy, and kidney failure are commonly reported complications of this disease. All of the AME patients reported until 1998 had the characteristic signs of severe AME. In 1998, the first patient with a mild form of AME who proved to have mutations that resulted in an HSD11B2 protein with attenuated activity was

reported (4). Only three clinical features of the mild AME are the same as in severe AME: low renin, low aldosterone, and elevated (THF+alloTHF)/THE ratio.

Following our initial description of the disease-causing mutation in the *HSD11B2* gene (5, 6), around 40 additional mutations have been described in less than 70 patients worldwide (Fig. 1A). Despite the small number of available patients, previous studies have documented correlations between genotype and phenotype (7, 8). For example, mutations that severely attenuate HSD11B2 activity, as assessed *in vitro,* cause severe disease, including early fatality, while mutations associated with mildly attenuated enzyme activity give rise to type 2 AME, often with a late-onset presentation of mild hypertension.

We recently published evidence for genotype–phenotype concordance in 1,507 families with congenital adrenal hyperplasia (CAH) due to 21-hydroxylase deficiency and 220 CAH patients with 11β-hydroxylase deficiency (9-11). In both studies, we used *in silico* dynamic modeling to define structural changes that each *CYP21A2* and *CYP11B1* mutation induces in the respective enzymes, namely 21-hydroxylase and 11β-hydroxylase. By correlating these changes with clinical phenotype, we defined structural derangements underpinning the clinical variants of CAH, namely salt-wasting, simple virilizing, and non-classical CAH (9). A previous attempt with AME mutations sought to correlate structure with function using a dimeric quaternary structure (12). This structure-function relationship is in contradiction with experimental evidence suggesting that the HSD11B2 monomer is, in fact, the active form of the enzyme (13).

In this study, we provide extensive data on the demographics, genotype, phenotype, and hormonal profile of 36 AME patients from our International Consortium for Rare Steroid Disorders, together with long-term outcomes in a subset. To evaluate genotype-structure-phenotype correlations, we constructed a 3D homology model of HSD11B2, to which we mapped all the known *HSD11B2* missense mutations, and additionally carried out molecular

dynamic simulations to understand alterations in structural flexibility. Thus, as with CAH, we present our prediction of disease severity based on mutation-induced changes in HSD11B2 structure. This *in silico* strategy, we believe, will facilitate the prediction of AME phenotype when new mutations are discovered.

RESULTS

We report the demographics and clinical phenotype of 36 genetically confirmed AME patients from the International Consortium of Rare Steroid Disorders. The majority of patients were of Omani (22/36) and Persian (6/36) descent, with 75% being from consanguineous marriages, mainly within Oman (Fig. 1B and Dataset S1). The median age of AME diagnosis was 4.6 years (range: 0.1-15) and the cohort was distributed equally for either sex. The majority of patients (86%) were born at term, with 76% being born small for gestational age. Fig. 1A shows that, in our cohort, there were 6 missense, 1 insertion, 2 deletion, and 3 frameshift mutations, and 2 indels. Expected from the pathophysiology of AME, the presenting mean arterial pressure was elevated above the 90^{th} percentile for all subjects (Fig. 1C). The average serum potassium level at diagnosis was low at 2.72 mmol/L (range: 1.5 to 4.1 mmol/L), while serum bicarbonate was high at 29.5 mmol/L (range: 20-38 mmol/L) (Figs. 1D and 1E). Serum aldosterone levels were expectedly low (Fig. 1F), with two patients with elevated levels due to unclear reasons. Additionally, renin levels were low, except for two patients (10.4 and 14 ng/mL/hr) that were on therapy (Table 1). In a subset of 29 patients, the average (THF + alloTHF)/THE ratio, representing the major urinary metabolites of cortisol and cortisone, was significantly elevated at 19 (range: 3-55, normal: 1.0) (Fig. 1G). Of note is that 27 of 36 (75%) patients also presented with nephrocalcinosis. The nephrocalcinosis may arise from chronic long-standing hypokalemia as noted, for example, in Bartter syndrome type III (14).

To understand whether the clinical phenotype of HSD11B2 deficiency could be predicted

by examining changes in enzyme structure induced by a given *HSD11B2* mutation, we performed *in silico* analytics using three estrogenic HSD17B1 [PDB id 1IOL (15), 1JTV (16), 1FDV (17)] that exhibited a 27% sequence similarity with HSD11B2 over 284 amino acids (Fig. S1A). The human HSD11B2 model exhibited a characteristic conserved NAD-binding Rossman Fold motif (Fig. S1B) with an adjacent substrate-binding site (Fig. S1C and S1D). 500 ns of molecular dynamics (MD) simulations of the monomer and dimeric forms of HSD11B2 indicated a stable model with stably folded protein (Figs. S1E to S1H). We used ICM software to determine ΔΔG of missense mutations found in AME patients or experimentally engineered mutations. All mutations (Fig. 2A) showed an increase in ΔΔG values, suggesting the loss of protein stability and function (Fig. 2B).

HSD11B2 exists as a homodimer in its inactive state (13). Four residues, namely, R186, E190, A237 and R336, lie at the dimer interface and could therefore interfere with dimer formation (Fig. 2C). Residues R186 and E190 are positioned at the dimer interface on the α4 helix. An inter-subunit ion-pair interaction (R186-E190) is formed as a result of the two-fold inverted symmetry of the adjacent subunit (Fig. 2D), akin to the R112-E120 ion pair in HSD17B1 (15-17). Importantly, this interaction was found to be stable, and was maintained throughout the course of 500 ns MD simulations (Figs. 2E, 2F and 2G). Furthermore, the interaction was found to stabilize the α4 helix and maintains flexibility around the coenzyme-binding site. Thus, the R186C mutation results in the loss of inter-subunit ion pair and pushes the equilibrium towards formation of an active monomeric enzyme (Fig. 2H). It also prevents the formation of the intra-helical ion pair interaction and thus permits the destabilization of structural elements around the coenzyme-binding site.

There are several other disruptive mutations at this dimer interface involving residues A237, D244, L251 and D176. The residue A237 is surrounded by L241 and V239 from both HSD11B2 subunits. Its mutation to Val enhances hydrophobicity of this cluster and strengthens

the enzyme's inactive dimeric state (Fig. 2I). The residue D244 not only creates an intra-subunit salt bridge with R336 that holds the α5 helix and β7 sheets together, but also hydrogen bond interactions with R360 from the adjacent subunit (Fig. 2J). Its mutation to Asn decreases the strength of the R360 interaction leading to the loss of the salt bridge with R366 – this, in turn, impairs protein stability. Similarly, mutation of a hydrophobic L251 side chain to hydroxyl group of Ser increases polarity and forms a hydrogen bond with the positively charged side chain groups of R360 – this enhances dimer binding (Fig. 2K). Finally, the mutation of D176 to Asn creates a hydrogen bond between asparagine and T200, thus enhancing the inactive dimer state (Fig. 2L).

Mutations of HSD11B2 residues which form the substrate or coenzyme (NAD^+) binding pocket have been shown in *in vitro* studies to eliminate enzyme activity (18) and cause severe AME. For example, Y226 is located in the substrate-binding pocket (Fig. 3A). The aromatic phenol side chain forms hydrophobic interactions with the aromatic ring of the substrate. The Y226N mutation replaces this residue with a non-aromatic residue resulting in the loss of hydrophobic stacking, which interferes with substrate binding (Fig. 3A). Furthermore, this mutation changes the side chain from being hydrophobic to hydrophilic, which is unfavorable for the binding of a hydrophobic substrate. The A221V mutation replaces the short side chain with a slightly bulkier side chain of Val, thus interfering with substrate binding by reducing the volume of the pocket, while the A221G mutation decreases hydrophobicity and introduces flexibility around the rigid binding pocket (Fig. 3B).

Our model shows that the polar 17-OH group in cortisol is tucked in a hydrophobic region surrounded by Y226, P227 and L229. This hydroxyl group is absent in corticosterone, which results in enhanced hydrophobic interactions and ~10-fold higher binding affinity to HSD11B2 compared with cortisol (Fig S2A). Besides the kidney, HSD11B2 is also expressed in the placenta. Although the mineralocorticoid receptor is not expressed in this tissue, HSD11B2

inactivates cortisol to eliminate its growth-inhibiting and pro-apoptotic effects during embryonic development. During pregnancy, the high level of progesterone in the maternal circulation can bind to and modulate HSD11B2 activity. This may translate into effects of any loss-of-function mutations that disrupt progesterone binding on birth weight. For example, the A221V mutation severely affects the binding of progesterone more than cortisol because of the steric clashes between Val and the projecting methyl groups in progesterone (Fig. S2B). Very interestingly, we find that the two patients with the A221V mutations were small for gestational age (Table 1). Likewise, the A221G mutation affects progesterone binding indirectly by altering the structure of the binding site. Similarly, the Y226N mutation is more detrimental to progesterone binding as it reduces hydrophobic interactions between the progesterone skeleton and the hydroxyphenyl ring of tyrosine (Fig. S2B). In contrast, P227 provides indirect structural support to the binding site, and mutation to Leu has similar affects for both cortisol and progesterone (Fig. S2B).

There are four mutations that reside in and disrupt the co-enzyme binding site, thus severely impairing HSD11B2 activity. The side chain of residue L179 is normally positioned spatially in a short turn between the β4 sheet and α4 helix (Fig. 3C). By allowing interactions with the hydrophobic side chains of V174 and L282, these interactions make the coenzyme-binding site more flexible. Mutation to Arg introduces a guanidinium side chain, which allows interactions with the carboxyl group side chain of E172 and the hydroxyl group side chain of T184 (Fig. 3C), thus introducing rigidity to the turn and decreasing the flexibility required for optimal enzyme function (7). Situated in the coenzyme binding pocket, Y232 is a highly conserved residue in the Rossman fold motif (19), suggesting that its mutation will be detrimental to enzyme activity (20). The hydroxyl-phenyl side chain of Y232 forms important hydrogen bonds with N171 and NAD^+, holding the coenzyme in correct position for its catalytic function (Fig. 3D). This interaction is disrupted in the Y232C mutation causing severe AME. The importance of this residue in enzyme activity has been independently confirmed by several

engineered mutations (20) (Fig. 3D). In the G89D mutation, the carboxyl side chain of Asp displays severe steric clashes with the ribose sugar moiety of adenosine, which affects the binding of NAD^+ (Fig. 3E). Another engineered mutation K236R leads to the disruption of NAD binding (Fig. 3F). While retaining the ability to interact with the NAD^+ through hydrogen bonding, the mutation abolishes enzyme activity (20).

Impairments in structural stability of HSD11B2 disrupt its tertiary structure causing a marked attenuation of enzyme activity and severe AME. The residue L250 is positioned in the α5 helix, and its side chains sit in a tight hydrophobic pocket surrounded by the side chains of L204, F246, W253, V255 and V257 (Fig. 4A). The hydrophobic pocket residues are locked by an ion-pair interaction between R208-E249. Introduction of a Pro side chain breaks the α5 helix by introducing rigidity, which prevents a large, bulky guanidinium side chain of Arg from being accommodated in the tight binding pocket (Fig. 4A). A subsequent loss of hydrophobicity in this region affects structural stability. Another stable intra-helical ion pair interaction is formed between D144 and R147 (Fig. 4B). This interaction allows the α3 helix to pack tightly with the adjacent β sheets near the NAD^+ binding site. The D144V mutation results in the loss of this interaction and destabilizes the packing arrangement (Fig. 4B). The hydrophobic packing is also disrupted in F185S mutation, when the aromatic side chain of phenylalanine, surrounded by hydrophobic residues of V182, C188 and M189, is replaced with a polar side chain of serine (Fig. 4C). Similarly, the hydrophobic side chain of L363, surrounded by M347, I350 and F362, is positioned in a helix-turn-helix (Fig. 4D). The L363P mutation disrupts the helix and the local structural environment.

Furthermore, several mutations can disrupt packing of the HSD11B2 protein to impair stability through the introduction of a bulkier residue. Residue A328 forms hydrophobic interaction with V215, I260, I325 and Y338 (Fig. 4E). By replacing the alanine with a bulkier Val

residue, the A328V mutation causes steric clashes with the side chain of I260 and Y338 from the surrounding β sheets (Fig. 4E). Residue S180 is positioned on a loop and its hydroxyl group side chain interacts with the side chain and backbone nitrogen of T184 (Fig. 4F). This side chain lies within a very constricted space and restricts the accommodation of any bulkier residue, which causes steric clashes, in fact, without altering the protein structure. Thus, a Phe side chain with a bulky aromatic ring, as in S180F mutation, is not tolerated at this position (Fig. 4F).

Multiple hydrogen bonds and salt bridges between polar residues stabilize the tertiary structure of the HSD11B2 enzyme. Certain mutations cause a loss of these interactions, resulting in inactive enzyme and severe AME. For example, the salt bridge between R208 and E249 is critical (Fig. 4G). Its loss, as in the case of the R208C and R208H mutations, destabilizes the protein and results in severe disease (Fig. 4G). Likewise, D223 forms a salt bridge with R337 (Fig. 4H). By replacing this salt bridge with a less strong bond, a hydrogen bond, the D223N mutation changes the negatively charged residue to an uncharged polar residue resulting in a marked attenuation of *in vitro* activity (21). This also suggests that the salt bridge plays a crucial role in maintaining HSD11B2 stability and activity. The side chains of R213 form hydrogen bonds with the backbone atoms of residues A331 and L329 (Fig. 4I). By diminishes these hydrogen bonds, which help maintain the tertiary structure of the protein, R213C mutation impairs enzyme stability (Fig. 4I).

The Arg/Tyr cluster from residues 335 to 339 has previously been implicated in maintaining protein stability, although precise mechanism has remained unclear (22). Mutations involving these residues have been reported in AME patients, including the R337C and Y338H. Simulations of the monomer and dimeric HSD11B2 models suggest that residue R337 forms a salt bridge interaction with D223 and hydrogen bonds with the OH group of Y339 (Fig. 4J). There interactions appear to be important in maintaining correct folding and stability of the

protein. Thus, its mutation to Cys abolishes both the salt bridge and hydrogen bond to destabilize the enzyme and cause severe AME. Genetically engineered mutations of this residue further show that R337K, which maintains polarity and positive charge, reduces enzyme activity by 70%, while R337A, which is similar to R337C in having uncharged and short side chains, inactivates HSD11B2 completely (Fig. 4J) (22). In the same Arg/Tyr cluster, mutation of Y338 to His inactivates the enzyme to cause severe AME. Our model suggests that this Tyr residue forms hydrophobic interactions with A328 and hydrogen bonds with D327 (Fig. 4K). Both interactions help sustain protein stability, so that the substitution of Tyr with His, for example, inactivates HSD11B2. This is because, although Y338H retains the hydrogen bonding ability, it has shorter side chains that destabilize the enzyme. Similarly, the substitution of Tyr with Phe in an engineered Y338F construct is not tolerated. Here, hydrophobic interactions are retained but hydrogen bonding is abolished (22). Finally, R337 and Y338 in the Arg/Tyr cluster are also highly conserved across many species; thus, any changes to these residues are unlikely to be tolerated (22).

Several mutations are reported to cause a milder form of AME with a less severe clinical and biochemical manifestations. The relevant mutated constructs were shown to have maintained HSD11B2 activity *in vitro* (4, 18, 23), consistent with the less severe clinical phenotype. Structurally, these mutations can either indirectly disrupt substrate binding (such as the P227L mutation in one of our patient) or alter protein structure (such as the R279C and R359W mutations) to attenuate, but not abolish enzyme activity (Fig. 5). Notably, while the P227 residue does not lie in a position that directly interacts with the substrate, its adjacent positioning to residue Y226 suggests that it may have a role in substrate binding (Fig. 5A). In fact, this residue forms the ‘kink’ in the loop region, maintaining the conformation of the active site and also holds Y226 in the correct position to optimally interact with the substrate. Mutation of this residue to Leu (P227L) disrupts the ‘kink’ and alters the positioning of Y226 (Fig. 5A).

Two non-conservative mutations thought to disrupt the tertiary structure of HSD11B2 have been identified in patients with AME type 2. R279 forms a hydrogen bond with the backbone of N171, which helps maintain and stabilize the local protein environment (Fig. 5B). Replacement of R279 by a residue that does not form a hydrogen bond, as in the R279C mutation, leads to mild attenuation, but not total elimination of HSD11B2 activity (23), consistent with a mild clinical phenotype (Fig. 5B). Another non-conservative mutation, R359W, changes the properties of the side chain from charged to hydrophobic. This alters the local interaction within the protein structure, in which the positively charged side chain of R359 forms a hydrogen bond with the backbone carbonyl oxygen of I350 (Fig. 5C). A loss of this interaction contributes towards the enhanced structural flexibility, causing attenuation of enzyme activity. Of note is that both R279C and R359W cause minimal disruption to the intramolecular interactions and occur near the surface of the protein.

DISCUSSION

AME is an extremely rare disorder, with less than one hundred cases reported to date (24). Most patients are found in populations where consanguinity and endogamy are common (25). The low prevalence of AME and the relatively limited number of mutations in the HSD11B2 enzyme have together rendered it difficult to study genotype-phenotype associations. Our consortium represents the largest AME cohort described phenotypically.

Of the 16 patients we have reported preliminarily (6, 8, 26-28), follow up data was available on 8 males and 6 females (6 to 26 years of age). Like CAH, height of the patients improved, but fell below the target height (height SDS: -1.1 ± 0.6). Cardiovascular complications were prominent, with three patients dying from cardiac arrest at 16, 16 and 17 years of age. Severe hypertension left ventricular hypertrophy (12/16) and hypertensive retinopathy (10/16) were prominent clinical features. For the 13 surviving patients with available

follow-up echocardiograms, 12 had persistent left ventricular hypertrophy, 3 showed aortic root dilation, and 2 had aortic insufficiency. Another notable clinical feature was nephrocalcinosis, which persisted in 8/9 patients at 4.1 to 14.5 years follow-up, despite treatment of hypokalemia. Four patients developed renal insufficiency more than 10 years after diagnosis, with two progressing to renal failure and received renal transplantation (29). Interestingly, following transplant, these patients no longer showed clinical signs of AME, with a remission of the low-renin hypertension and hypokalemic alkalosis when medical treatment with spironolactone was discontinued.

On follow-up, three females conceived spontaneously. One patient had 2 miscarriages prior to a viable pregnancy that she carried to term. Spironolactone was discontinued due to non-compliance, which resulted in severe hypertension and renal failure. The second patient carried her pregnancy to term, with spironolactone being discontinued in the first trimester and ensuing blood pressure control with methyldopa. The third patient was treated with eplerenone and hydrochlorothiazide during pregnancy; she had severe hypertension (BP: 217/91) associated with preeclampsia at 24 weeks of gestation and delivered a nonviable fetus. This long-range follow up of an ultra-rare disorder has profound implications on the future management of newly discovered AME patients.

The role of the mineralocorticoid receptor and the HSD11B2 enzyme in essential hypertension is being increasingly recognized. The presentation of the mild form of AME mimics essential hypertension as there are no electrolyte abnormalities. Mild mutations were identified in patients with mild clinical markers of AME, namely, low aldosterone, hypertension, and abnormal ratio of cortisol to cortisone and *in vitro* studies demonstrated a very mild alteration in enzyme activity (6, 23). The mild form is best identified by mutations in the *HSD11B2* gene as other hallmarks, such as low birth weight, poor growth, severe hypertension and hypokalemia, are absent. Increased (THF+alloTHF)/THE ratios have also been reported in

16 to 32% of essential hypertension, consistent with HSD11B2 dysfunction (30, 31). Furthermore, treatment with mineralocorticoid receptor antagonists has been shown to lower blood pressure in patients with essential hypertension, heart failure and hypertension resistant to conventional antihypertensives (32-34). For a subset of patients with low renin-low aldosterone hypertension, mineralocorticoid receptor antagonists may be the most effective therapy. HSD11B2 enzyme deficiency also accelerates atherogenesis and causes proinflammatory changes in the endothelium of mouse models; this is reduced by eplerenone (35). Polymorphisms of the HSD11B2 gene have been associated with hypertension (36). Despite these overlaps between clinical features of mild AME and essential hypertension, the most definitive diagnosis of the former is by genetic diagnosis.

One of the main factors contributing to the development of hypertension is the amount of salt intake. Nevertheless, not all individuals respond to a salt load in the same way; notably, some develop hypertension while others do not. AME is a form of salt-sensitive monogenic hypertension. In addition to expression in the kidney, HSD11B2 is also expressed in the *brain*. Brain-specific *Hsd11b2* knockout mice show increased salt appetite and salt sensitivity (37). It has been suggested that minor abnormalities of this enzyme may explain salt-sensitivity in the pathogenesis in essential hypertension.

Early reports suggested that changes in the structural integrity of HSD11B2 can cause severe AME, whereas intronic mutations that yield mildly impaired enzyme could result in type 2 disease (38). To this end, correlations between clinical phenotype and the magnitude of reduction in enzymatic activity *in vitro* for certain mutations have been described (7). Nonetheless, precise structural changes induced by specific mutations have *hitherto* remained unsolved. A prior *in silico* model has used the dimeric quaternary structure, but it was later shown experimentally that the active form of HSD11B2 was, in fact, the monomer (12, 13).

Here, we report the successful identification, by computational modeling, of structural changes *in silico* that are induced by HSD11B2 mutations. We have used this analysis to provide structural explanations for the effect of mutations on HSD11B2 function. We find that mutations that cause severe AME are those that enhance dimerization, disrupt the substrate- or coenzyme-binding site, or severely impair structural stability. We have also categorized mutations that result in a mild AME (type 2) phenotype, namely P227L, R279C and R359W, as those indirectly disrupting substrate binding or causing mild alterations in protein structure.

Based on observations from the humanized model, we find that most of the mutations occur in yet uncharacterized regions of the HSD11B2 protein. We thus employed molecular dynamic (MD) simulations in explicit solvent on both monomeric and dimeric models to understand the structural flexibility of these residues. We conclude that HSD11B2 mutations exert their effect by disrupting intra-molecular interactions, which alter protein structure and impair structural stability. Of these mutations, those that affect multiple salt bridge interactions, hydrogen bond networks and hydrophobic patches have a greater impact on disrupting overall structural integrity. In contrast, mutations that only affect a single intra-molecular interaction, such as R279C and R359W, cause relatively minor disruptions, and are, therefore, more tolerated. This is because loss of a single interaction is likely to be compensated by interactions formed between other residues.

The analysis presented here is based on a given missense mutation affecting the HSD11B2 protein. However, in the case of compound heterozygosity, we would expect the resulting clinical phenotype to result from the combined effects of two mutations. As an example, a patient presenting with mild AME (type 2) was a compound heterozygote having inherited two HSD11B2 mutations (18). As one of the mutations, Y232C, occurred at the coenzyme-binding site, we predict on basis of our *in silico* categorization, that it would severely attenuate enzymatic activity. However, the other mutation, L376P (residues beyond residue

369), is expected to result in HSD11B2 with sufficient residual activity. The resulting mild clinical phenotype is therefore consistent with only 50% of near-normal functioning enzyme. In yet another example, despite inheriting two mutations expected to result in severely attenuated HSD11B2, the patient did not present with AME until 21 years of age (18). There is no ready explanation for this, but it is known that minimal residual enzyme activity might just be sufficient for mineralocorticoid escape.

Overall, therefore, we infer that there is close concordance between the structural disruption of HSD11B2 caused by a given mutation and the resulting clinical phenotype. We have recently performed a similar exhaustive *in silico* analysis for the ~150 known mutations affecting the steroidogenic enzyme 21-hydroxylase (9). Almost all mutations were categorized in terms of specific patterns of structural changes that correlated tightly with the three known clinical phenotypes of congenital adrenal hyperplasia (CAH), namely salt wasting, simple virilizing and non-classical CAH. For example, if the mutation was located within 5Å of the substrate- or heme-binding site, the outcome invariably was salt-wasting CAH, whereas if non-conserved hydrophobic patches were disrupted, the disease was a milder, simple virilizing variety.

Our *in silico* categorization of clinical severity of mutations can potentially be used to predict clinical severity or phenotype of new mutations very early during gestation, particularly with the availability of prenatal diagnostic testing. To this end, using patients from our CAH cohort, we can now establish, as early as 6 weeks of gestation, whether the fetus is affected or a carrier by Next Generation Sequencing of free fetal DNA in the mother's plasma (39). Our *in silico* prediction tool, together with this new technology, should change the paradigm for "early" prenatal diagnosis of a variety of autosomal recessive disorders, including AME.

METHODS

The cohort of AME patients, which was a part of the International Consortium of Rare Steroid Disorders (Principal Investigator: Maria I. New), was recruited independently in 7 countries by pediatric endocrinologists, with appropriate Institutional Review Board (IRB) or Ethics Committee approval. Genotyping was performed by PCR at Mount Sinai or at overseas institutions using appropriate primer sets, as described previously (6, 28). Serum potassium, bicarbonate and aldosterone, and urinary THF and THE levels were measured locally at commercial laboratories. The methods for computational modeling, including molecular dynamic modeling, are found in the Supplementary Methods section and in Haider et al (9).

ACKNOWLEDGMENTS

The authors sincerely acknowledged the summer studentship funding support from the Biochemical Society and the Nuffield Trust, and the support from the National Institutes of Health: Grants AG40132, AG23176, AR65932, DK113627 and AR67066 (to M.Z).

REFERENCES

1. Krozowski ZS & Funder JW (1983) Renal mineralocorticoid receptors and hippocampal corticosterone-binding species have identical intrinsic steroid specificity. *Proc Natl Acad Sci U S A* 80(19):6056-6060.
2. Arriza JL*, et al.* (1987) Cloning of human mineralocorticoid receptor complementary DNA: structural and functional kinship with the glucocorticoid receptor. *Science* 237(4812):268-275.
3. New MI, Levine LS, Biglieri EG, Pareira J, & Ulick S (1977) Evidence for an unidentified steroid in a child with apparent mineralocorticoid hypertension. *J Clin Endocrinol Metab* 44(5):924-933.
4. Wilson RC*, et al.* (1998) A genetic defect resulting in mild low-renin hypertension. *Proc Natl Acad Sci U S A* 95(17):10200-10205.
5. Agarwal AK, Rogerson FM, Mune T, & White PC (1995) Gene structure and chromosomal localization of the human HSD11K gene encoding the kidney (type 2) isozyme of 11 beta-hydroxysteroid dehydrogenase. *Genomics* 29(1):195-199.
6. Wilson RC*, et al.* (1995) A mutation in the HSD11B2 gene in a family with apparent mineralocorticoid excess. *J Clin Endocrinol Metab* 80(7):2263-2266.
7. Nunez BS*, et al.* (1999) Mutants of 11beta-hydroxysteroid dehydrogenase (11-HSD2) with partial activity: improved correlations between genotype and biochemical phenotype in apparent mineralocorticoid excess. *Hypertension* 34(4 Pt 1):638-642.
8. Dave-Sharma S*, et al.* (1998) Examination of genotype and phenotype relationships in 14 patients with apparent mineralocorticoid excess. *J Clin*

Endocrinol Metab 83(7):2244-2254.

9. Haider S*, et al.* (2013) Structure-phenotype correlations of human CYP21A2 mutations in congenital adrenal hyperplasia. *Proc Natl Acad Sci U S A* 110(7):2605-2610.
10. Khattab A*, et al.* (2017) Clinical, genetic, and structural basis of congenital adrenal hyperplasia due to 11beta-hydroxylase deficiency. *Proc Natl Acad Sci U S A* 114(10):E1933-E1940.
11. New MI*, et al.* (2013) Genotype-phenotype correlation in 1,507 families with congenital adrenal hyperplasia owing to 21-hydroxylase deficiency. *Proc Natl Acad Sci U S A* 110(7):2611-2616.
12. Manning JR, Bailey MA, Soares DC, Dunbar DR, & Mullins JJ (2010) In silico structure-function analysis of pathological variation in the HSD11B2 gene sequence. *Physiol Genomics* 42(3):319-330.
13. Gomez-Sanchez EP*, et al.* (2001) The 11beta hydroxysteroid dehydrogenase 2 exists as an inactive dimer. *Steroids* 66(11):845-848.
14. Watanabe T & Tajima T (2005) Renal cysts and nephrocalcinosis in a patient with Bartter syndrome type III. *Pediatr Nephrol* 20(5):676-678.
15. Azzi A*, et al.* (1996) Crystal structure of human estrogenic 17 beta-hydroxysteroid dehydrogenase complexed with 17 beta-estradiol. *Nat Struct Biol* 3(8):665-668.
16. Gangloff A, Shi R, Nahoum V, & Lin SX (2003) Pseudo-symmetry of C19 steroids, alternative binding orientations, and multispecificity in human estrogenic 17beta-hydroxysteroid dehydrogenase. *FASEB J* 17(2):274-276.

17. Mazza C, Breton R, Housset D, & Fontecilla-Camps JC (1998) Unusual charge stabilization of NADP+ in 17beta-hydroxysteroid dehydrogenase. *J Biol Chem* 273(14):8145-8152.

18. Lavery GG*, et al.* (2003) Late-onset apparent mineralocorticoid excess caused by novel compound heterozygous mutations in the HSD11B2 gene. *Hypertension* 42(2):123-129.

19. Agarwal AK, Rogerson FM, Mune T, & White PC (1995) Analysis of the human gene encoding the kidney isozyme of 11 beta-hydroxysteroid dehydrogenase. *J Steroid Biochem Mol Biol* 55(5-6):473-479.

20. Obeid J & White PC (1992) Tyr-179 and Lys-183 are essential for enzymatic activity of 11 beta-hydroxysteroid dehydrogenase. *Biochem Biophys Res Commun* 188(1):222-227.

21. Carvajal CA*, et al.* (2003) Two homozygous mutations in the 11 beta-hydroxysteroid dehydrogenase type 2 gene in a case of apparent mineralocorticoid excess. *J Clin Endocrinol Metab* 88(6):2501-2507.

22. Atanasov AG*, et al.* (2007) Impaired protein stability of 11beta-hydroxysteroid dehydrogenase type 2: a novel mechanism of apparent mineralocorticoid excess. *J Am Soc Nephrol* 18(4):1262-1270.

23. Li A*, et al.* (1998) Molecular basis for hypertension in the "type II variant" of apparent mineralocorticoid excess. *Am J Hum Genet* 63(2):370-379.

24. Morineau G*, et al.* (2006) Apparent mineralocorticoid excess: report of six new cases and extensive personal experience. *J Am Soc Nephrol* 17(11):3176-3184.

25. Quinkler M*, et al.* (2004) Molecular basis for the apparent mineralocorticoid

excess syndrome in the Oman population. *Mol Cell Endocrinol* 217(1-2):143-149.

26. Lin-Su K*, et al.* (2004) In vitro expression studies of a novel mutation delta299 in a patient affected with apparent mineralocorticoid excess. *J Clin Endocrinol Metab* 89(5):2024-2027.

27. Obeyesekere VR*, et al.* (1995) The R337C mutation generates a high Km 11 beta-hydroxysteroid dehydrogenase type II enzyme in a family with apparent mineralocorticoid excess. *J Clin Endocrinol Metab* 80(11):3381-3383.

28. Wilson RC*, et al.* (1995) Several homozygous mutations in the gene for 11 beta-hydroxysteroid dehydrogenase type 2 in patients with apparent mineralocorticoid excess. *J Clin Endocrinol Metab* 80(11):3145-3150.

29. Khattab AM, Shackleton CH, Hughes BA, Bodalia JB, & New MI (2014) Remission of hypertension and electrolyte abnormalities following renal transplantation in a patient with apparent mineralocorticoid excess well documented throughout childhood. *J Pediatr Endocrinol Metab* 27(1-2):17-21.

30. Campino C*, et al.* (2010) 11beta-Hydroxysteroid dehydrogenase type-2 and type-1 (11beta-HSD2 and 11beta-HSD1) and 5beta-reductase activities in the pathogenia of essential hypertension. *Endocrine* 37(1):106-114.

31. Mongia A*, et al.* (2012) Role of 11betaHSD type 2 enzyme activity in essential hypertension and children with chronic kidney disease (CKD). *J Clin Endocrinol Metab* 97(10):3622-3629.

32. Savoia C, Touyz RM, Amiri F, & Schiffrin EL (2008) Selective mineralocorticoid receptor blocker eplerenone reduces resistance artery stiffness in hypertensive patients. *Hypertension* 51(2):432-439.

33. Pitt B*, et al.* (1999) The effect of spironolactone on morbidity and mortality in patients with severe heart failure. Randomized Aldactone Evaluation Study Investigators. *N Engl J Med* 341(10):709-717.

34. Vaclavik J*, et al.* (2011) Addition of spironolactone in patients with resistant arterial hypertension (ASPIRANT): a randomized, double-blind, placebo-controlled trial. *Hypertension* 57(6):1069-1075.

35. Deuchar GA*, et al.* (2011) 11beta-hydroxysteroid dehydrogenase type 2 deficiency accelerates atherogenesis and causes proinflammatory changes in the endothelium in apoe-/- mice. *Endocrinology* 152(1):236-246.

36. Mariniello B*, et al.* (2005) Analysis of the 11beta-hydroxysteroid dehydrogenase type 2 gene (HSD11B2) in human essential hypertension. *Am J Hypertens* 18(8):1091-1098.

37. Evans LC*, et al.* (2016) Conditional Deletion of Hsd11b2 in the Brain Causes Salt Appetite and Hypertension. *Circulation* 133(14):1360-1370.

38. Mune T, Rogerson FM, Nikkila H, Agarwal AK, & White PC (1995) Human hypertension caused by mutations in the kidney isozyme of 11 beta-hydroxysteroid dehydrogenase. *Nat Genet* 10(4):394-399.

39. New MI*, et al.* (2014) Noninvasive prenatal diagnosis of congenital adrenal hyperplasia using cell-free fetal DNA in maternal plasma. *J Clin Endocrinol Metab* 99(6):E1022-1030.

FIGURE LEGENDS

Figure 1: Clinical Profile for Patients with Apparent Mineralocorticoid Excess (AME) Due to 11β-Hydroxysteroid Dehydrogenase Type 2 Deficiency from 7 Nations of the International Consortium for Rare Steroid Disorders. (A) Structure of the human *HSD11B2* gene that contains 5 exons, showing known mutations and those harbored by 36 patients in this international cohort (bold). **(B)** Worldwide distribution of our cases of 11β-hydroxysteroid dehydrogenase type 2 deficiency. Mean arterial blood pressure **(C)**, and serum potassium **(D)**, bicarbonate **(E)** and aldosterone **(F)** levels in our patient cohort shown as a function of age. Urinary tetrahydrocortisol (THF) plus allo-THF to tetrahydrocortisone (THE) [(THF+alloTHF)/THE ratio] **(G)** is shown for each genotype. Bold lines show the 90th percentile (C), or upper (E) or lower (D, F) limits of normal ranges. Filled red and blue circles, respectively, represent females and males with overt AME; red open circle represents a female with AME type 2.

Figure 2: Disruptive Mutations Affecting the Dimer Interface of HSD11B2. (A) Human HSD11B2 dimer model constructed using existing HSD17B1 crystal structures: 1IOL (co-crystallized with 17β-estradiol) that was the most complete structure, with no missing residues; 1JTV (1.5Å) that was co-crystallized with testosterone and exhibited higher resolution over 1IOL (2.3Å); and 1FDV that was co-crystallized with the coenzyme NAD. The positions of all known mutated residues are indicated. **(B)** $\Delta\Delta G$ values for severe (red) or mild (black) *HSD11B2* mutations. **(C)** At the dimer interface, two R186-E190 ion pairs are formed between the two-fold inverted symmetry of the adjacent subunits. In case of the monomer **(D)**, an intra-helical ion pair is formed, which is similar to the R112 and E120 salt bridge formed in the HSD17B1 templates. **(E)** Spatial positions of mutations (blue) mapped on one subunit. The two subunits

are distinctly colored (brown and blue). NAD^+ (yellow) and cortisol (green) are illustrated as sticks. The ion pair interaction at the dimer interface is stable throughout the 500 ns simulation **(F)**. However, some fluctuation is observed in the intra-helical interaction due to conformational changes in the monomer **(G)**. **(H)** R186 makes ion pair interactions with E190 from adjacent subunit. The R186C mutation results in the loss of the ion pair interaction. An intra-helical ion pair formed between R186-E190 in the monomer is also lost. **(I)** A237V mutation enhances hydrophobicity at the interface. **(J)** D244 forms an intra-subunit ion pair interaction with R336, as well as hydrogen bonds with R360 from the adjacent subunit. The polar uncharged side chain of asparagine in the mutant is unable to provide structural stability. **(K)** The OH group in the L251S mutation makes a hydrogen bond with R361 from the adjacent subunit, thus enhancing the interaction at the dimer interface. **(L)** The hydrogen bond formed between D176N and T200 enhances the inactive dimer state.

Figure 3: Interference with Coenzyme or Substrate Binding to HSD11B2. **(A)** The tyrosine at position 226 forms the wall of the substrate-binding site and imparts hydrophobicity. A mutation to N226 results in loss of hydrophobic stacking rendering it unfavorable for substrate binding. **(B)** A221V mutation reduces the volume of the substrate-binding pocket, while A221G increased flexibility around the binding site. **(C)** In the L179R mutation, the positively charged guanidinium side chain makes hydrogen bonds with the size chains of T184 and E172, thereby reducing the flexibility around the NAD^+-binding site. **(D)** The hydroxy-phenyl side chain of Y232 makes hydrogen bonds with the hydroxyl group of ribose sugar and side chain of N171. These hydrogen bonds are essential, as mutations to phenylalanine, serine or cysteine are not tolerated. The mutation to phenylalanine removes the hydroxyl group and leads to loss of the hydrogen bond, whereas mutation to serine with a shorter side chain results in increased distance of OH group from the NAD^+, and again prevents effective hydrogen bonding – both

mutations result in inactive enzyme. **(E)** The carboxyl side chain of aspartic acid in the G89D mutation causes severe steric clashes with the ribose sugar moiety of adenosine in NAD and affects coenzyme binding. **(F)** The bulkier side chain in K236R mutation decreases the size of the coenzyme-binding pocket. This is because the Arg residue with a bulkier side chain decreases the size of the coenzyme pocket, making it unfavorable for optimal NAD^+ binding.

Figure 4: Mutations Affecting HSD11B2 Stability. **(A)** L250 is positioned on α5 helix and the side chain is surrounded in a constricted hydrophobic pocket. A mutation to bulky arginine or proline that introduces helix distortion is not tolerated. **(B)** The D144V mutation results in the loss of the D144-R147 ion pair interaction and destabilizes the α3 helix packing arrangement near the NAD-binding site. **(C)** The polar side chain in F185S mutation disrupts the hydrophobic packing formed by V182, C188 and M189. **(D)** The hydrophobic L363 residue is positioned in a helix-turn-helix, surrounded by M347, I350 and F362. Mutation to proline disrupts the helix and the local structural environment. **(E)** In the A328V mutant, the side chain of valine displays steric clashes within the hydrophobic pocket. **(F)** The hydroxyl group side chain of S180 makes interactions with the backbone atoms and the side chain of T184. A phenylalanine side chain abolishes these interactions and imparts flexibility to the loop. **(G)** R208-E249 ion pair interactions hold α4 and α5 helices together. R208H/C mutants are unable to form this interaction. **(H)** The carboxyl side chain of D223 makes hydrogen bonds with the side chains of Q261 and R337. Mutation to Asn disrupts the hydrogen bond with R337. **(I)** The R213C mutation results in the loss of hydrogen bond interactions formed between the arginine side chain and the backbone atoms of A331 and L329**.** **(J)** R337 makes an ion pair interaction with D223 and also a hydrogen bond with Y339. While the lysine side chain retains decreased ability to form hydrogen bond with Y339, a mutation to histidine, cysteine, or alanine completely abolishes the R337-D223 ion pair interaction. **(K)** The hydroxy-phenyl side chain of Y338

makes hydrogen bond with the backbone atoms of D327 and A328. These interactions maintain the spatial positions of α7 and β7. A mutation to histidine or phenylalanine results in the loss of these interactions and introduces flexibility.

Figure 5: HSD11B2 Mutations Causing Mild AME Type 2. **(A)** P227 forms a 'kink' in the loop and helps to correctly position Y226 to optimally interact with the substrate. An increase in flexibility of the loop in the P227L mutation results in misalignment of Y226. **(B)** The hydrogen bond between R279 and N171 is one of many that hold β4 and β6 sheets together. It also orients the side chain of N171 to interact with NAD^+. Mutation to cysteine results in the loss of these interactions. **(C)** R359-I350 interactions maintain the helix-turn-helix. The R359W mutation introduces flexibility to the region.

Figure 1

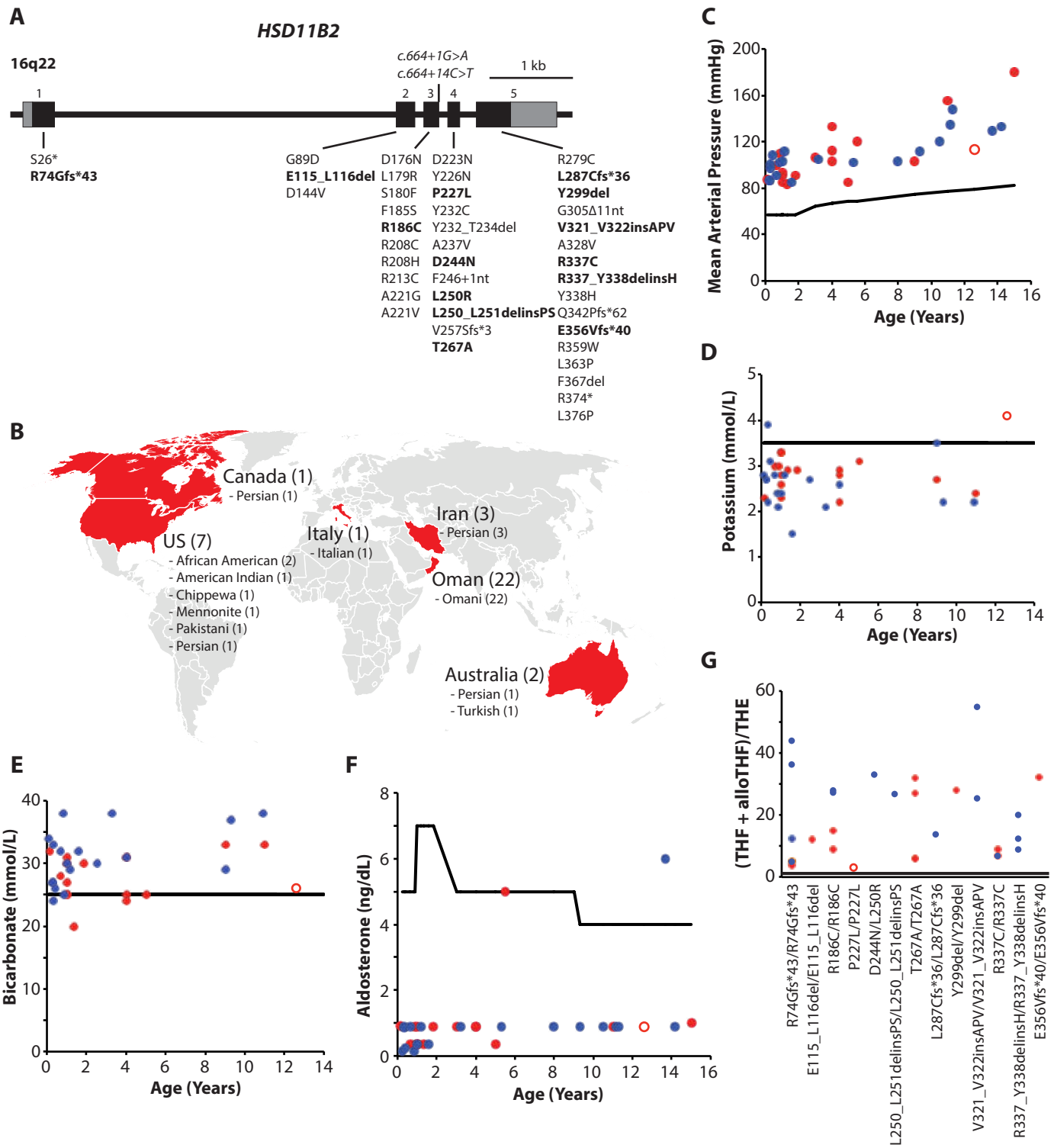
A
HSD11B2
16q22
c.664+1G>A
c.664+14C>T
1 kb
1
2
3
4
5
S26*
R74Gfs*43
G89D
E115_L116del
D144V
D176N
L179R
S180F
F185S
R186C
R208C
R208H
R213C
A221G
A221V
D223N
Y226N
P227L
Y232C
Y232_T234del
A237V
D244N
F246+1nt
L250R
L250_L251delinsPS
V257Sfs*3
T267A
R279C
L287Cfs*36
Y299del
G305Δ11nt
V321_V322insAPV
A328V
R337C
R337_Y338delinsH
Y338H
Q342Pfs*62
E356Vfs*40
R359W
L363P
F367del
R374*
L376P
B
Canada (1)
- Persian (1)
US (7)
- African American (2)
- American Indian (1)
- Chippewa (1)
- Mennonite (1)
- Pakistani (1)
- Persian (1)
Italy (1)
- Italian (1)
Iran (3)
- Persian (3)
Oman (22)
- Omani (22)
Australia (2)
- Persian (1)
- Turkish (1)
C
Mean Arterial Pressure (mmHg)
Age (Years)
D
Potassium (mmol/L)
Age (Years)
E
Bicarbonate (mmol/L)
Age (Years)
F
Aldosterone (ng/dL)
Age (Years)
G
(THF + alloTHF)/THE
R74Gfs*43/R74Gfs*43
E115_L116del/E115_L116del
R186C/R186C
P227L/P227L
D244N/L250R
L250_L251delinsPS/L250_L251delinsPS
T267A/T267A
L287Cfs*36/L287Cfs*36
Y299del/Y299del
V321_V322insAPV/V321_V322insAPV
R337C/R337C
R337_Y338delinsH/R337_Y338delinsH
E356Vfs*40/E356Vfs*40

Figure 2

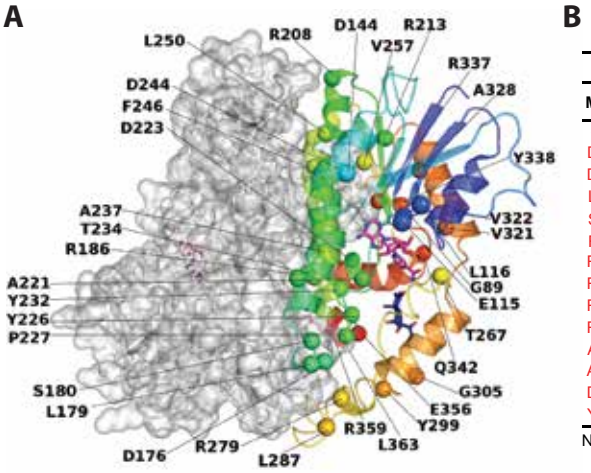

B

Disease				Engineered			
Mutant	ΔΔG (kcal/mol)	Mutant	ΔΔG (kcal/mol)	Mutant	ΔΔG (kcal/mol)	Mutant	ΔΔG (kcal/mol)
G89D	0.5	P227L	0.3	D91N	1.6	Y338H	1.8
D144V	1.7	Y232C	3.8	E115G	3.3	Y338A	2.7
D176N	2.1	A237V	0.8	E115K	2.6	Y338F	0.6
L179R	0.5	D244N	1.1	Y232F	1.0	Y339A	3.3
S180F	1.2	L250R	2.3	K236R	0.3	Y339H	1.8
F185S	1.5	L250P	3.2	R335K	2.2	Y339F	0.8
R186C	4.2	L251S	0.4	R335Q	1.6		
R208H	1.7	T267A	0.4	R335A	2.6		
R208C	4.8	R279C	4.1	R336K	1.2		
R213C	4.8	A328V	0.7	R336A	1.3		
A221V	0.4	R337C	2.8	R336Q	2.4		
A221G	1.3	Y338H	2.9	R337K	4.1		
D223N	1.0	R359W	4.0	R337A	2.8		
Y226N	2.0			R337Q	3.0		

Not studied: L363P, L376P

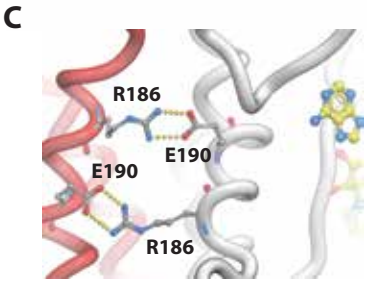

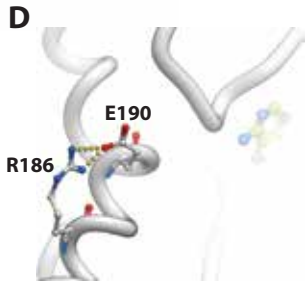

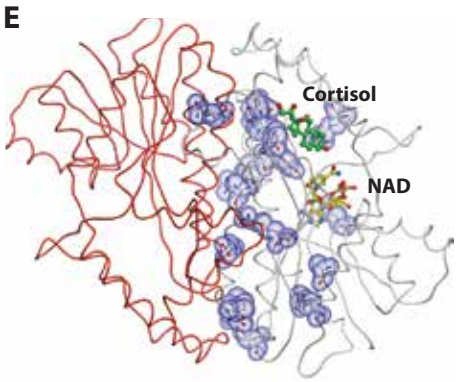

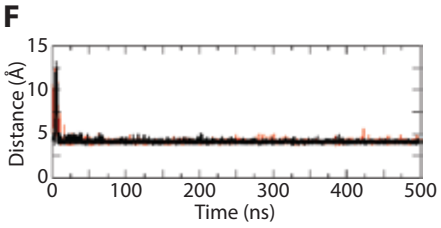

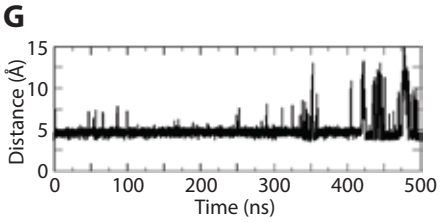

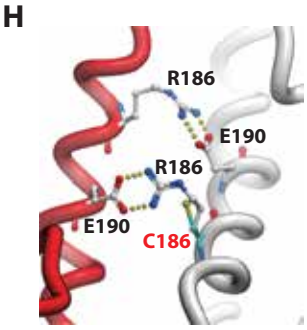

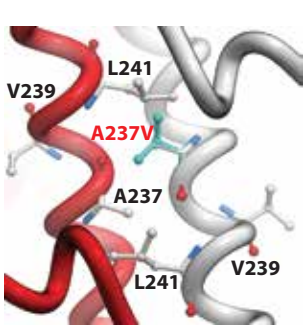

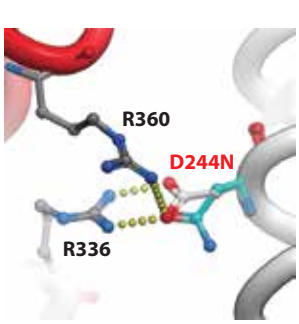

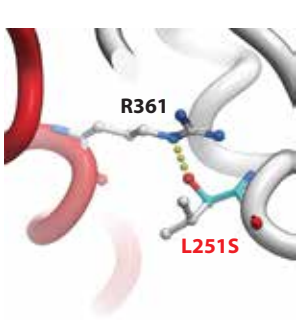

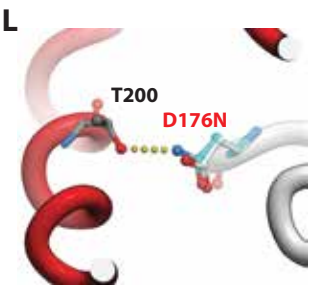

Figure 3

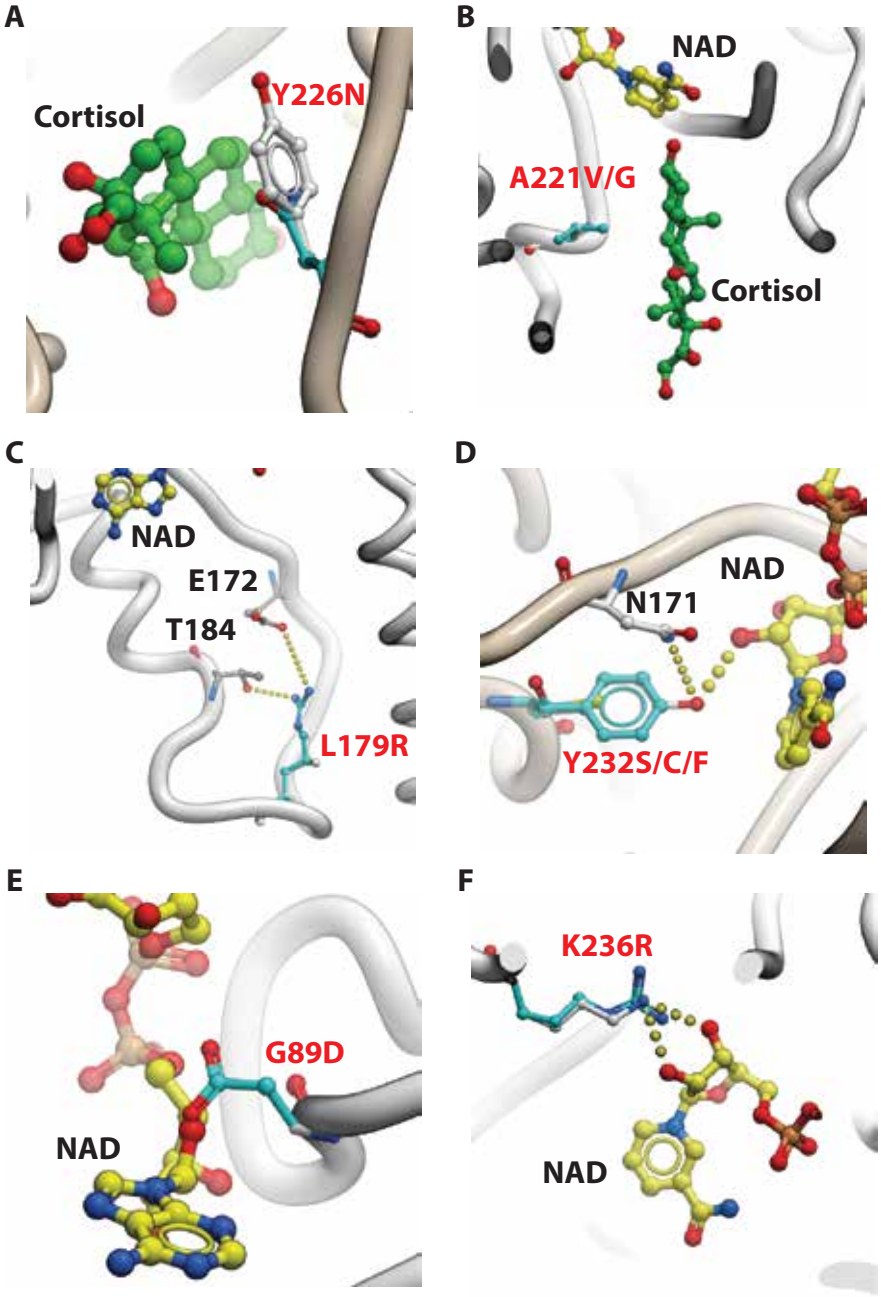
A
Cortisol
Y226N
B
NAD
A221V/G
Cortisol
C
NAD
E172
T184
L179R
D
NAD
N171
Y232S/C/F
E
G89D
NAD
F
K236R
NAD

Figure 4

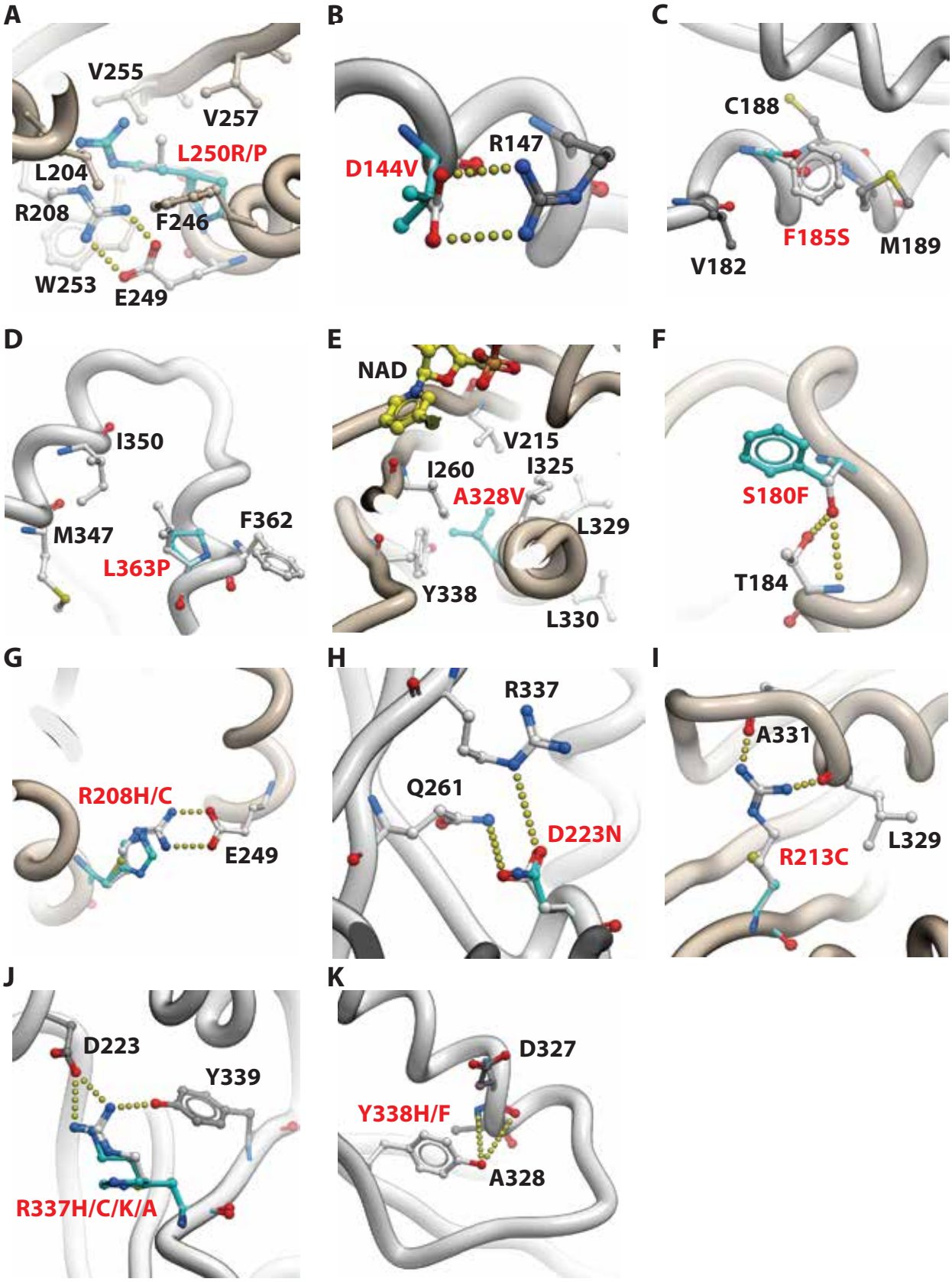
A
V255
V257
L250R/P
L204
R208
F246
W253
E249
B
D144V
R147
C
C188
F185S
M189
V182
D
I350
M347
F362
L363P
E
NAD
V215
I260
I325
A328V
L329
Y338
L330
F
S180F
T184
G
R208H/C
E249
H
R337
Q261
D223N
I
A331
L329
R213C
J
D223
Y339
R337H/C/K/A
K
D327
Y338H/F
A328

Figure 5

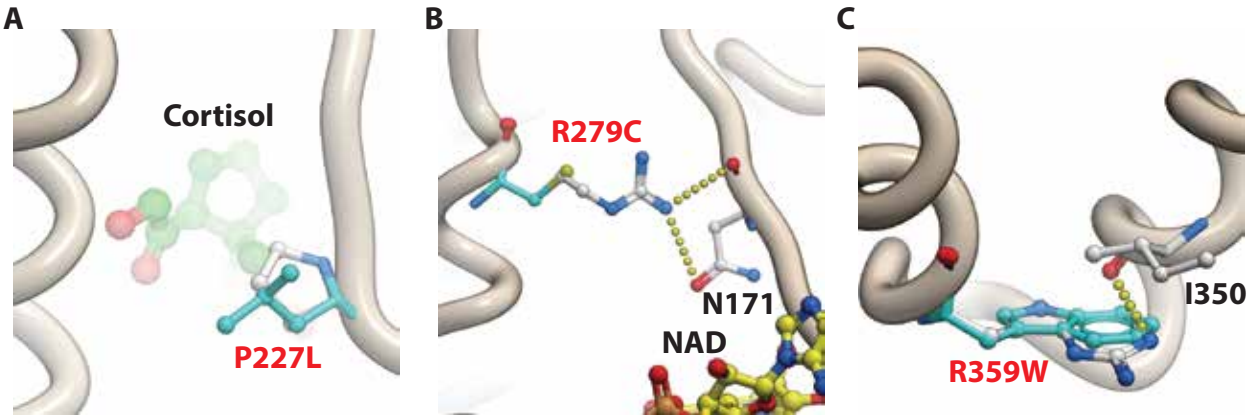

Table 1: Clinical Information of Patients with Apparent Mineralocorticoid Excess Reported in This Study

Patient ID	Sex	Gestational Age (Weeks)*	Birth Weight (kg)	Small for Gestational Age	Ethnicity	Consanguinity	Age at diagnosis (Years)	Systolic Pressure (mmHg)	Diastolic Pressure (mmHg)	Mean Arterial Pressure (mmHg)	Mean Arterial Pressure (90th percentile for age)	Serum Potassium (mM)	Serum Bicarbonate (mM)	Serum Aldosterone (ng/dL)	Plasma Renin Activity (ng/mL/hr)	(THF+5αTHF)/ THE	Nephrocalcinosis	Genotype
524	M	40	1.9	Y	US (Chippewa)	Y	11.1	180	112	134.7	77.7	2.1	38	<1	0.03	26.8	N	L250_L251delinsPS/L250_L251delinsPS
1054	M	40	2.3	Y	Italian	N	10.5	170	95	120.0	76.3	2.6	31	<1	0.08	33.0	Y	D244N/L250R
1058	F	40	2.1	Y	US (African American)	N	9.0	130	90	103.3	74.7	2.7	33		0.30	8.9	Y	R186C/R186C
1061	M	40	2.3	Y	US (Persian)	N	5.3	140	83	102.0	69.3	2.7	30	<1	0.12	12.5	N	R337_Y338delinsH/R337_Y338delinsH
1063	F	40	2.6	N	US (African American)	N	4.0	142	98	112.7	66.7	2.8	31		<0.12	14.9	Y	R186C/R186C
1101	F	40	2.4	Y	Iranian	Y	5.5	160	100	120.0	68.3			5	0.11	6.7	N	R337C/R337C
1105	M	40	2.1	Y	Iranian	Y	13.7	170	110	130.0	79.7			6	0.07	6.9	N	R337C/R337C
1107	F	40	2.2	Y	Iranian	Y	15.0	220	160	180.0	82.3			1	7.90	8.9	N	R337C/R337C
1262	M	40	2.0	Y	Omani	N	11.3	175	134	147.7	77.7	2.3	38	<1	0.47	27.9	Y	R208C/R208C
1265	M	40	2.0	Y	Omani	N	9.3	147	94	111.7	75.0	2.2	37	<1	0.40	27.3	Y	R208C/R208C
1278	M	40	2.0	Y	Australian (Persian)	Y	14.2	170	115	133.3	81.3	3.5	29	<1	7.90	9.0	Y	R337_Y338delinsH/R337_Y338delinsH
1416	M	40	2.0	Y	Canadian (Persian)	N	8.0	130	90	103.3	74.0	2.4	38	<1	0.07	20.1	Y	R337_Y338delinsH/R337_Y338delinsH
1567	F	term	3.6	N	US (Mennonite)	Y	12.6	160	90	113.3	78.7	4.1	26	<1	0.70	3.0	N	P227L/P227L
2500	M	40	2.5	Y	Australian (Turkish)	N	3.2	143	86	105.0	63.3	2.8	34	<1	0.06	13.8	Y	L287Cfs*36/L287Cfs*36
5390	F	36	2.0	N	US (Pakistani)	Y	11.0	225	120	155.0	77.3	2.4	33	<1	0.64	28.0	Y	Y299del/Y299del
9968	F	36	2.0	N	Omani	Y	0.9	150	90	110.0	57.0	3.0	28	<1	<0.15	3.8	Y	R74Gfs*43/R74Gfs*43
12629	F	term	2.0	Y	Omani	Y	1.3	110	70	83.3	57.0	2.9	20	0.37	14.00		Y	A221V/A221V
12630	F	term	2.0	Y	Omani	Y	1.0	115	70	85.0	57.0	3.3	25	0.37	0.20		Y	A221V/A221V
12633	M	40	1.8	Y	Omani	Y	1.0	156	76	102.7	55.3	2.4	30	0.37	0.20	25.5	Y	V321_V322insAPV/V321_V322insAPV
12634	F	40	2.1	Y	Omani	Y	0.7	138	80	99.3	57.0	3.0	28	0.37	0.20		Y	V321_V322insAPV/V321_V322insAPV
12637	M	36	1.9	Y	Omani	Y	0.4	150	87	108.0	55.3	3.1	26	0.25	0.20	44.0	Y	R74Gfs*43/R74Gfs*43
12640	F	term	2.0	Y	Omani	Y	0.1	123	70	87.7	57.0	2.3	32	0.93	<0.2	5.0	Y	R74Gfs*43/R74Gfs*43
12643	M	term	2.2	Y	Omani	Y	0.3	145	78	100.3	55.3	2.2	33	0.87	10.70		Y	R74Gfs*43/R74Gfs*43
12645	M	36	2.2	N	Omani	Y	1.2	155	90	111.7	55.3	2.8	29	<1		55.0	Y	V321_V322insAPV/V321_V322insAPV
12646	M	term	2.0	Y	Omani	Y	0.8	146	80	102.0	55.3	2.1	25	0.16	0.90		Y	T267A/T267A
12649	M	term	2.3	Y	Omani	Y	1.6	115	70	85.0	55.3	1.5	32	0.37	0.50	36.4	Y	R74Gfs*43/R74Gfs*43
12650	M	term	2.2	Y	Omani	Y	0.3	120	70	86.7	55.3	2.7	27	0.16	0.20		N	R74Gfs*43/R74Gfs*43
12653	M	term	2.2	Y	Omani	Y	0.7	116	79	91.3	55.3	2.8	32	<1	<0.2	5.1	Y	R74Gfs*43/R74Gfs*43
12654	M	34	1.5	N	Omani	Y	0.3	151	70	97.0	55.3	3.9	24	<1	0.20	12.5	Y	R74Gfs*43/R74Gfs*43
12657	F	term	2.9	N	Omani	Y	1.0	125	74	91.0	57.0	2.6	31	<1	<0.2	31.8	Y	T267A/T267A
12659	F	term	2.3	Y	Omani	Y	1.8	120	77	91.3	57.0	2.9	30	<1	<0.2	12.2	Y	E115_L116del/E115_L116del
12662	F	term	1.9	Y	Omani	Y	5.0	140	58	85.3	68.3	3.1	25	0.37	0.20		Y	T267A/T267A
12663	F	term	2.9	N	Omani	Y	1.0	120	80	93.3	57.0	2.8	27	0.37		6.1	N	T267A/T267A
12664	F	term	2.6	N	Omani	Y	4.0	135	87	103.0	66.7	2.9	25	<1		27.0	Y	T267A/T267A
12665	F	term	2.3	Y	Omani	Y	4.0	184	108	133.3	66.7	2.2	24	<1	<0.2	5.9	Y	T267A/T267A
12803	F	40	1.8	Y	US (American Indian)	N	3.0	140	90	106.7	64.0	2.3	30	<1	0.14	32.1	N	E356Vfs*40/E356Vfs*40

*term: 36-40 weeks of gestation; Patient with Type 2 AME shown in red.

SUPPLEMENTARY METHODS

The amino acid sequence for human HSD11B2 was obtained from UniProt (accession no. P80365) and used to search for homologous proteins in the Protein Data Bank. The top searches identified three estrogenic 17β-hydroxysteroid dehydrogenase-1 (HSD17B1) templates [PDB id 1IOL, 1JTV, 1FDV (15-17)]. Multiple sequence alignment was carried out using ClustalX (37). Models were constructed using the Internal Coordinate Mechanics method implemented in the Molsoft ICM software (38). The spatial position of coenzyme and ligand were retained in their respective binding sites. This was based on the assumption that the ligands and coenzyme interact in the similar manner and replicate all conserved interactions from the template into the model. Several rounds of energy minimization yielded a final low-energy conformation with no steric clashes between side chains. The final model, which accounts for residues 81-369, was chosen based on a low Cα rmsd overlap between the HSD17B1 templates and the humanized model (0.11Å, 0.15Å, 0.21Å with 1IOL, 1JTV and 1FDV respectively). Stereo chemical properties were evaluated using PROCHECK version 3.5.4 (39).

HSD11B2 is a member of the short-chain dehydrogenase/reductase protein family, which exhibit highly conserved coenzyme and ligand binding domains. High conservation in the overall fold between HSD17B1 and HSD11B2 permitted the adoption of structural features of the template into the model. The 1FDV structure has been crystallized with NAD^+ coenzyme. A large ligand-binding pocket located adjacent to the coenzyme-binding site accommodates estradiol (1IOL) and testosterone (1JTV) in two different orientations. The natural substrate of HSD11B2, cortisol, was docked in the ligand-binding pocket using the docking suite of the ICM software (38).

Models were initially generated as monomers. Dimers were created after superimposition of the monomers on the two-fold inverted-symmetry related half of the

monomer in the 1IOL template. Monomeric and the dimeric forms of HSD11B2 were subjected to restraint-free atomistic molecular dynamics simulations for 500ns each to (a) test the stability of the models and (b) understand the structural role of mutations at the dimer interface. AMBER ff99SB-ILDN force field was used to describe the systems (40). The force field parameters for NAD were obtained from the AMBER parameter database (41). The coordinates for cortisol were sketched and minimized in the ICM software (38) and parameterized using the Antechamber program (42). The systems were solvated using TIP3P water molecules in a box of size 75 x 69 x 81 $Å^3$ (monomer) and 104 x 69 x 81 $Å^3$ (dimer), whose boundaries extended at least 10Å from the edge of the solute. Counter ions were added to neutralize the charges. Equilibration was carried out in two phases employing 10ns each of isothermal-isochoric (NVT) ensemble using a Langevin thermostat set at 300K and isothermal-isobaric (NPT) ensemble using a Berendsen barostat set at 1atm, hydrogen mass portioning and a time step of 4 fs. The final production run was carried out till 500ns. ACEMD (43) was the preferred choice of MD engine, running on NVIDIA GTX780 GPUs. All analysis was carried out using the AMBER suite of programs (44).

Molecular graphics images were generated using the ICM browser (38). A list of currently known missense mutations, their corresponding clinical features and enzyme activity were extracted and cross-evaluated from various original publications.

LEGENDS TO SUPPLEMENTARY FIGURES

Figure S1: The Human HSD11B2 Model. (A) Sequence alignment between the human HSD17B1 templates (PDB id 1FDV, 1IOL, 1JTV) and HSD11B2 sequence. Conserved residues are highlighted green, and partial conservation within the same amino acid family is highlighted in yellow. The sequence similarity between the templates and HSD11B2 sequence is 27%. **(B)** HSD11B2 coenzyme-binding site. NAD^+ (yellow sticks) is surrounded by 20 amino acids and includes T88, G89, D91, S92, F94, V113, L114, M137, D138, L139, T140, N167, V191, N192, V217, S219, Y232, K236, F265 and F267. **(C)** Docking of cortisol to the HSD11B2 model. The substrate-binding site (blue mesh) lies adjacent to the NAD^+-binding site (yellow sticks). The volume of the cavity is 412 $Å^3$, as identified by the pocket finder program in the ICM suite. **(D)** HSD11B2 substrate-binding site. Cortisol (green sticks) is surrounded by 14 residues and includes N171, S219, Y226, C228, L229, Y232, C264, F307, S310, L311, L344, Q364, F367 and I368. RMSD plots of Cα atoms in monomer **(E)** and individual monomers in the dimeric **(F)** models over 500 ns molecular dynamic (MD) simulation run, as well as radius of gyration (Rg) plots of the monomer **(G)** and individual monomers in the dimeric **(H)** models. These plots highlight the structural stability of HSD11B2.

Figure S2: Interaction of HSD11B2 with Corticosterone and Progesterone. (A) During the simulations, the 17-OH group in cortisol (green) is tucked in a hydrophobic region surrounded by the aromatic ring of Y226, P227, and the side chains of L229. This polar 17-OH group is not present in corticosterone (cream) and might contribute to enhanced hydrophobic interactions around this hydrophobic region. **(B)** A221V/G mutation lie in the vicinity of the 19-methyl group of progesterone. Additionally, Y226N and P227L mutations are also likely to influence the differential binding of progesterone

(purple) and cortisol (green). This is due to the slight changes in the structure of progesterone and cortisol and the orientation in which they bind in the active site.

Figure S1

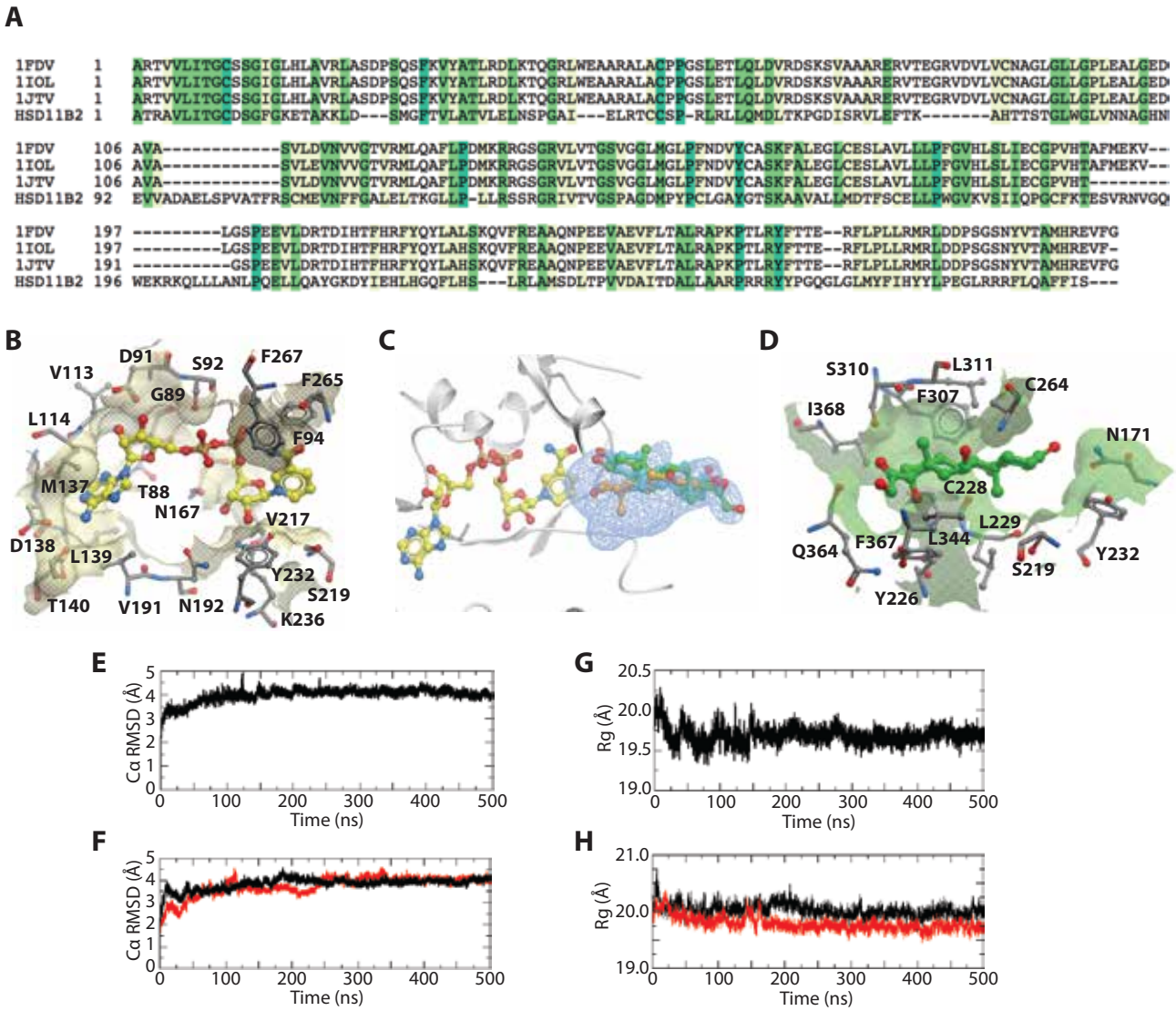
A
1FDV 1 ARTVVLITGCSSGIGLHLAVRLASDPSQSFKVYATLRDLKTQGRLWEAARALACPPGSLETLQLDVRDSKSVAAARERVTEGRVDVLVCNAGLGLLGPLEALGED
1IOL 1 ARTVVLITGCSSGIGLHLAVRLASDPSQSFKVYATLRDLKTQGRLWEAARALACPPGSLETLQLDVRDSKSVAAARERVTEGRVDVLVCNAGLGLLGPLEALGED
1JTV 1 ARTVVLITGCSSGIGLHLAVRLASDPSQSFKVYATLRDLKTQGRLWEAARALACPPGSLETLQLDVRDSKSVAAARERVTEGRVDVLVCNAGLGLLGPLEALGED
HSD11B2 1 ATRAVLITGCDSGFGKETAKKLD---SMGFTVLATVLELNSPGAI---ELRTCCSP-RLRLLQMDLTKPGDISRVLEFTK-------AHTTSTGLWGLVNNAGHN
1FDV 106 AVA----------SVLDVNVVGTVRMLQAFLPDMKRRGSGRVLVTGSVGGLMGLPFNDVYCASKFALEGLCESLAVLLLPFGVHLSLIECGPVHTAFMEKV--
1IOL 106 AVA----------SVLEVNVVGTVRMLQAFLPDMKRRGSGRVLVTGSVGGLMGLPFNDVYCASKFALEGLCESLAVLLLPFGVHLSLIECGPVHTAFMEKV--
1JTV 106 AVA----------SVLDVNVVGTVRMLQAFLPDMKRRGSGRVLVTGSVGGLMGLPFNDVYCASKFALEGLCESLAVLLLPFGVHLSLIECGPVHT--------
HSD11B2 92 EVVADAELSPVATFRSCMEVNFFGALELTKGLLP-LLRSSRGRIVTVGSPAGDMPYPCLGAYGTSKAAVALLMDTFSCELLPWGVKVSIIQPGCFKTESVRNVGQ
1FDV 197 ---------LGSPEEVLDRTDIHTFHRFYQYLALSKQVFREAAQNPEEVAEVFLTALRAPKPTLRYFTTE--RFLPLLRMRLDDPSGSNYVTAMHREVFG
1IOL 197 ---------LGSPEEVLDRTDIHTFHRFYQYLAHSKQVFREAAQNPEEVAEVFLTALRAPKPTLRYFTTE--RFLPLLRMRLDDPSGSNYVTAMHREVF-
1JTV 191 ----------GSPEEVLDRTDIHTFHRFYQYLAHSKQVFREAAQNPEEVAEVFLTALRAPKPTLRYFTTE--RFLPLLRMRLDDPSGSNYVTAMHREVFG
HSD11B2 196 WEKRKQLLLANLPQELLQAYGKDYIEHLHGQFLHS---LRLAMSDLTPVVDAITDALLAARPRRRYYPGQGLGLMYFIHYYLPEGLRRRFLQAFFIS---
B
V113
D91
S92
F267
F265
G89
L114
F94
M137
T88
N167
V217
D138
L139
Y232
S219
T140
V191
N192
K236
C
D
S310
L311
C264
F307
I368
N171
C228
L229
Q364
F367
L344
Y232
S219
Y226
E
Cα RMSD (Å)
Time (ns)
F
Cα RMSD (Å)
Time (ns)
G
Rg (Å)
Time (ns)
H
Rg (Å)
Time (ns)

Figure S2

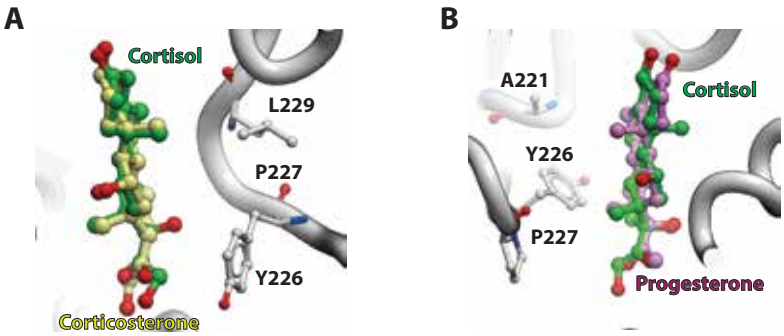
A
Cortisol
L229
P227
Y226
Corticosterone
B
A221
Cortisol
Y226
P227
Progesterone